Nucleation, growth, and coarsening for two- and three-dimensional phase transitions

Giridhar Madras[a,*], Benjamin J. McCoy[b]

[a]*Department of Chemical Engineering, Indian Institute of Science, Bangalore 560 012, India*
[b]*Department of Chemical Engineering, Louisiana State University, Baton Rouge, LA 70803, USA*

Abstract

Phase transitions from a metastable state often occur by nucleation accompanied by particle growth and eventually by Ostwald coarsening. In closed systems, the supersaturation declines as particles nucleate and grow, causing an increase in the stable critical nucleus size. Particles below the critical size dissolve spontaneously during coarsening and their mass is released to contribute to further growth of remaining particles. By developing a population balance model that represents nucleation, growth, and coarsening, we here determine the dynamics of particle size distributions (PSDs). The governing equations are solved numerically to show that the transition from nucleation and growth to coarsening occurs over a relatively long time period. The asymptotic coarsening stage reveals a power-law increase in average particle mass as the PSD evolves to a (minimum) polydispersity index of unity for both two-dimensional (2-D) and 3-D phase transitions. The model agrees with published conclusions that nucleation and coarsening overlap when interfacial energy is small or supersaturation is large.

Keywords: A1. Computer simulations; A1. Crystal growth and dissolution; A1. Crystal size distributions; A1. Growth models; A1. Moment and numerical solutions; A1. Population balance equations

1. Introduction

Nucleation, growth, and coarsening constitute three basic processes in condensation phase transition [1], where particles nucleate, grow, and eventually form a single condensed ripened particle. In a metastable supersaturated phase, nuclei

*Corresponding author. Tel.: +91 080 309 2321; fax: +91 080 360 0683.
E-mail addresses: giridhar@chemeng.iisc.ernet.in (G. Madras), bjmccoy@lsu.edu (B.J. McCoy).

will be generated and will also contribute to the growth of particles [2–4]. With the decrease of supersaturation due to growth, the size of the critical nucleus increases and the driving force for growth decreases. The Gibbs–Thomson effect and Ostwald coarsening become significant as the growth and nucleation rates decline. When particles shrink to their critical nucleus size, they become thermodynamically unstable and spontaneously disintegrate [5,6] so that the particle distribution narrows. After a very long time, the particle size distribution (PSD) approaches a delta distribution of zero variance with a single remaining particle at equilibrium [5]. The theory of coarsening has its origins in the work of Ostwald [7], Lifshitz and Slyozov [8], and Wagner [9] (LSW), as outlined by Dunning [10] and Mullins [11]. Applications to two-dimensional (2-D) systems began at least 40 years ago [12] and continue to be an active area of research.

The model developed here quantitatively describes this complete range of phenomena for both 2-D and 3-D systems. Much of the discussion that follows applies to both 2-D and 3-D systems, unless specifically noted otherwise. The sequence of reversible condensation processes is mathematically similar to reversible polymerization–depolymerization by monomer addition–dissociation [13]. Written for the PSD, the population balance equation (PBE) for a batch system (closed to flow) has an accumulation (time derivative) term, addition and dissociation terms, and a source (or sink) to represent nucleation (or denucleation). An expansion [14] of the PBE, for small ratio of monomer to particle mass, converts the difference-differential equation into a Fokker–Planck equation conventionally applied to Ostwald coarsening [1]. This approach has already been applied to investigate coarsening dynamics in our previous publications [5,6,15,16]. The particle distribution approximates an exponential self-similar solution, and eventually narrows until but one large particle remains, satisfying the mass balance. The long-time asymptotic result for the numerical solution of the scaled PBE shows a power-law decrease of particle number and a power-law growth of average particle mass, $C^{\mathrm{avg}}(\theta)$. The asymptotic power-law growth with time θ, $C^{\mathrm{avg}} \sim \theta^{1/(1-\lambda+1/d)}$, is determined by the dimension d and the power law for the mass in rate coefficient expressions. Experimentally observed coarsening behavior can thus be quantitatively represented by choosing λ for a given time range.

As described above, the decomposition of a supersaturated solid solution by precipitation of a new phase is often supposed to occur in three distinct steps: nucleation, growth and coarsening. Traditionally, these three processes have often been considered separate from each other with the implicit assumption that one process goes to completion before the next process begins. However, recent theories by Kampmann and Wagner [17], Robson [18] and our previous studies [5,6] have shown that nucleation, growth, and coarsening significantly overlap; thus, the time evolution of the particle number density and size depends on the rates of all three processes. While many models predict the evolution of the mean precipitate parameters like size and radius, we have developed models, similar to the Kampmann and Wagner [17,18] numerical (KWN) model, capable of predicting the full evolution of the size distribution. We use a population balance model to describe the evolution of the PSD through the first appearance of nuclei, subsequent monomer deposition and growth, and eventual coarsening to a single large remaining particle. Though some models [16,17,19,20] account for denucleation by allowing the particles above the critical size to shrink gradually, we consider that particles of size less than the critical nucleus size are unstable and disintegrate instantaneously and spontaneously into the monomer phase. This provides a rational and predictable way to reduce the particle population until a single large particle exists for $t \to \infty$, as dictated by Ostwald coarsening [1,21]. The theory shows the time evolution of the PSD for all times, and matches the LSW theory [8,9] in its restricted long-time range. Further, the classical LSW theory of coarsening applies only in the regime where the mean and critical radii are equal. When the size of a particle is smaller than the critical size, however, it will disintegrate and disappear from the PSD. This may occur well before the onset of the conditions that lead to LSW coarsening, and both

the KWN and our theory incorporate this effect into the model.

The KWN model and the proposed model determine the time evolution of the PSD using mean field approximations for rates. Though the general limitations of disregarding spatial inhomogeneous diffusion fields are well known [22], attempts at avoiding mean-field theories are mostly restricted to a few particles. By approaching the problems based on distribution kinetics, we describe properties of the time-dependent PSD that may be difficult to compute by other methods. Indeed, the model can incorporate some inhomogeneities such as allowing for distributions consisting of a large particle surrounded by small particles [15]. The capture number (defined as the mean rate of capture of diffusing adatoms by islands), the local environment of a particle, and particle mobility all influence the evolution of the PSD, but have limited influence on the essential behavior of the average island size and number density [15]. The validity of predictions suggests that the capability of a theory to quantify the PSD evolution is more important than avoiding the mean field approximation.

The KWN model has successfully predicted precipitate evolution in a wide range of model alloy systems [23–25], including Cu–Co, Ni–Al, Al–Sc and Fe–Ni. These predictions, in conjunction with experimental evidence, confirm that for certain alloys and heat treatment conditions, there is an overlap of nucleation and coarsening, as discussed by Robson [18]. In contrast to the modified KWN model [18], the distribution kinetics model can describe systems with high precipitate volume fractions [26] (by including interactions between particles) and the effect of temperature [27]. We have applied this approach separately to investigate nucleation with growth [28], Ostwald coarsening [6], transition [29] in 3-D, and the effect of temperature on these processes [27,30]. For a fixed temperature, analysis of the nucleation and growth equations show that the three most critical system-dependent variables are the interfacial energy, supersaturation, and solute diffusivity. The model provides a simple yet effective and powerful tool for systematically analyzing the effect of supersaturation, diffusivity, and interfacial energy on nucleation, growth and coarsening. In addition, the size-independent, diffusion-controlled and surface-controlled processes can be represented by simply choosing the value on the power on mass in rate coefficient as 0, $\frac{1}{3}$, and $\frac{2}{3}$, respectively.

The objective of this paper is (a) to develop the phase transition dynamics for a 2-D system based on the theory developed earlier [27] for 3-D systems, and (b) to compare the results obtained by the theory to that obtained by the modified KWN model [18]. The paper develops and evaluates these concepts in the following sections. Section 2 uses the capillarity approximation [2] to represent homogeneous nucleation kinetics and distribution kinetics to model the transition from growth to Ostwald coarsening. Section 3 describes the numerical scheme for solving the PBEs for the supersaturation and PSD evolution and discusses the results obtained. Section 4 presents a summary and the major conclusions.

2. Theory

The 2- or 3-D size distributions are defined by $c(x,t)\mathrm{d}x$, representing the area or volume concentration of particles at time t in the differential mass range $(x,\ x+\mathrm{d}x)$. Moments [31] are defined as integrals over the mass,

$$c^{(n)}(t) = \int_0^\infty c(x,t)x^n\,\mathrm{d}x. \tag{2.1}$$

The zeroth moment, $c^{(0)}(t)$, and the first moment, $c^{(1)}(t)$, are the time-dependent number and mass concentration of particles, respectively. The ratio of the zeroth and first moments is the average particle mass, $c^{\mathrm{avg}} = c^{(1)}/c^{(0)}$. The polydispersity, c^{pd}, defined as $c^{(2)}c^{(0)}/(c^{(1)})^2$, is a measure of the breadth of the distribution.

Reversible addition of monomer, $\mathbf{M}(x_\mathrm{m})$, to a particle, $\mathbf{C}(x)$, with rate coefficients, $k_\mathrm{g}(x)$ and $k_\mathrm{d}(x)$, for growth and dissolution, respectively, is represented by

$$\mathbf{C}(x) + \mathbf{M}(x_\mathrm{m}) \underset{k_\mathrm{d}(x)}{\overset{k_\mathrm{g}(x)}{\rightleftarrows}} \mathbf{C}(x+x_\mathrm{m}). \tag{2.2}$$

The distribution of the particles, $c(x,t)$, is governed by the kinetic equation (population balance),

$$\begin{aligned}\partial c(x,t)/\partial t &= -k_g(x)c(x,t)\int_0^\infty m(x',t)\,dx' \\ &+ \int_0^x k_g(x-x')c(x-x',t)m(x',t)\,dx' \\ &- k_d(x)c(x,t) \\ &+ \int_x^\infty k_d(x')c(x',t)\delta(x-(x'-x_m))\,dx' \\ &+ I\delta(x-x^*). \end{aligned} \tag{2.3}$$

The distribution of monomers, $m(x,t) = m^{(0)}(t)\,\delta(x-x_m)$, for a closed system with no input of monomer evolves according to

$$\begin{aligned}\partial m(x,t)/\partial t &= -m(x,t)\int_0^\infty k_g(x')c(x',t)\,dx' \\ &+ \int_x^\infty k_d(x')c(x',t)\delta(x-x_m)\,dx' \\ &- I\delta(x-x^*)x^*/x_m, \end{aligned} \tag{2.4}$$

where nucleation of critical nuclei of mass x^* at the rate I uses a number of monomers equal to x^*/x_m. The distribution changes according to Eq. (2.3), which becomes, when the integrations over the Dirac distributions are performed, the finite-difference integrodifferential equation,

$$\begin{aligned}\partial c(x,t)/\partial t &= -k_g(x)c(x,t)m^{(0)} + k_g(x-x_m)c(x-x_m,t)m^{(0)} \\ &- k_d(x)c(x,t) + k_d(x+x_m)c(x+x_m,t) \\ &+ I\delta(x-x^*). \end{aligned} \tag{2.5}$$

The governing equations show that $c(x,t)$ increases by addition and decreases by the loss of mass x_m. Eq. (2.5) can be expanded for $x_m \ll x$ to convert the differences into differentials.

Microscopic reversibility for the growth process implies

$$k_d(x) = m_{eq}^{(0)} k_g(x) \tag{2.6}$$

and we assume the growth rate increases as a power of mass,

$$k_g(x) = \gamma x^\lambda. \tag{2.7}$$

Thus, the mass dependences of the growth and dissolution rate coefficients are identical with $\lambda = 0, \frac{1}{3}, \frac{2}{3}$ representing various deposition rates. The power is $\lambda = \frac{1}{3}$ for diffusion-controlled and $\lambda = \frac{2}{3}$ for surface-controlled processes [32–34].

In 3-D the nucleus energy is the sum of interfacial and volume terms,

$$W_3(r) = 4\pi r^2\sigma - (\tfrac{4}{3})\pi r^3\varepsilon. \tag{2.8}$$

Here, $\varepsilon = (\rho/x_m)k_B T \ln S$ is expressed in terms of mass density ρ, monomer mass x_m, the Boltzmann constant k_B, and absolute temperature T, and σ is the interfacial energy between the condensed phase of the disk and the free monomers on the substrate. The term $-k_B T \ln S$ is the chemical potential difference between the two phases in terms of supersaturation S. The maximum energy occurs at $r^* = 2\sigma/\varepsilon$, or in terms of the spherical-particle mass, $x^* = (\frac{4}{3})\pi r^{*3}\rho$,

$$\xi_3^* = x^*/x_m = (\omega_3/\ln S)^3, \tag{2.8a}$$

where $\omega_3 = (\sigma/k_B T)(32x_m^2\pi/3\rho^2)^{1/3}$.

For two dimensions we consider disk-shaped islands of height h and radius r (Fig. 1), which have volume $\pi r^2 h$ and curved edge surface area $2\pi rh$. The island mass is $x = \rho\pi r^2 h$. Because only surface processes are being considered, only the edge effects are important energetically and the energies associated with the top and bottom surfaces can be neglected. The combined surface and volume energies provide

$$W_2(r) = 2\pi rh\sigma - \pi r^2 h\varepsilon. \tag{2.9}$$

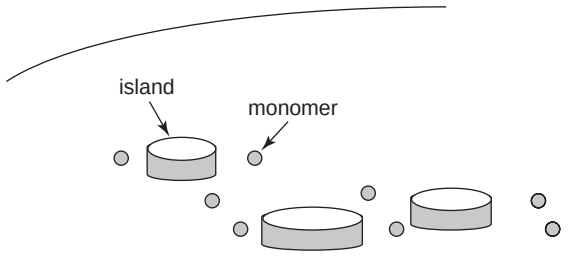

Fig. 1. Schematic of 2-D islands (disks) on a surface with monomers.

The maximum energy according to Eq. (2.9) is at the radius r^*,

$$r^* = \sigma/\varepsilon \tag{2.10}$$

or

$$\xi_2^* = (\omega_2/\ln S)^2,$$

where

$$\omega_2 = (\sigma/k_B T)(x_m \pi h/\rho)^{1/2}. \tag{2.10a}$$

For either 2- or 3-D, we can generalize and write

$$\xi_d^* = (\omega_d/\ln S)^d \tag{2.10b}$$

in terms of the dimension d.

Classical nucleation theory accounts for particle growth by means of the particle energy, W. For a supersaturated (metastable) 3-D system, the energy of a particle of radius r, $W(r)$, reaches a maximum value, W^*, at the critical particle radius, r^*, given by Eq. (2.8), and equivalent to the Gibbs–Thomson equation,

$$W_3^* = \left(\tfrac{16}{3}\right)\pi\sigma^3/\varepsilon^2. \tag{2.11}$$

For 2-D, one obtains the maximum energy expression,

$$W_2^* = h\pi\sigma^2/\varepsilon. \tag{2.12}$$

For $r<r^*$ (or in terms of mass, $x<x^*$), the energy W increases with size, implying that the particle is unstable and subject to fluctuations that dissociate most particles to monomer. For $r>r^*$, the energy decreases with size and the particle can grow or dissolve by diffusive or other stable, reversible kinetic mechanisms. By analogy with Eqs. (2.8) and (2.9), for an 1-D system, there is no interface curvature and the first term for W is independent of size; hence, no maximum energy exists, and nucleation, denucleation, and Ostwald coarsening would not occur. To generalize, we have for the nucleus energy,

$$W_d^*/k_B T = \omega_d^d (\ln S)^{1-d}/(d-1), \tag{2.13}$$

which reduces to the expression derived earlier for 3-D systems [6]. Strain energy can be incorporated into the expression for excess free energy of a cluster, but because the effects cannot be experimentally verified [35], they are neglected in this model.

The classical expression [2,36] for the nucleation rate (moles of nuclei/vol · time) is the flux over the maximum energy barrier (at $r = r^*$),

$$I_{nuc} = k_{nuc} \exp(-W^*/k_B T) \tag{2.14}$$

with a prefactor that varies with the square of monomer concentration, and thus with the square of the supersaturation, S^2. We will consider the prefactor as a parameter for the computations described below.

Dimensionless quantities are defined as

$$\begin{aligned} &\xi = x/x_m, \;\; \theta = t\gamma m_\infty^{(0)} x_m^\lambda, \;\; S = m^{(0)}/m_\infty^{(0)}, \\ &C = c x_m/m_\infty^{(0)}, \;\; C^{(n)} = c^{(n)}/(m_\infty^{(0)} x_m^n), \\ &J = I/(\gamma (m_\infty^{(0)})^2 x_m^\lambda), \end{aligned} \tag{2.15}$$

where ξ is the number of monomers in a particle. The scaled time θ, particle distribution C, nucleation rate J, and monomer concentration S, are scaled by the monomer concentration, $m_\infty^{(0)}$, in equilibrium with an uncurved surface.

The dimensionless monomer equation is

$$\mathrm{d}S(\theta)/\mathrm{d}\theta = [-S(\theta) + e^{\Omega_a}]C^{(\lambda)} - J\xi^*. \tag{2.16}$$

Because Eq. (2.16) is a moment equation, Ω_a is evaluated for the average-sized particle, $\Omega_a = \omega_d/(C^{avg})^{1/d}$. Exact for an infinitely narrow distribution, this approximation has been shown to be reasonable in previous computations [6] for crystal growth and Ostwald coarsening. The mass balance, $\mathrm{d}(S + C^{(1)})/\mathrm{d}\theta = 0$, is always satisfied,

$$S(\theta) = S_0 + C_0^{(1)} - C^{(1)}(\theta), \tag{2.17}$$

which can be substituted into Eq. (2.5) to give the dimensionless equation for C,

$$\begin{aligned} &\partial C(\xi,\theta)/\partial\theta \\ &= [S_0 + C_0^{(1)} - C^{(1)}(\theta)][-\xi^\lambda C(\xi,\theta) \\ &\quad + (\xi-1)^\lambda C(\xi-1,\theta)] - \xi^\lambda \exp(\omega\xi^{-1/d}) C(\xi,\theta) \\ &\quad + (\xi+1)^\lambda \exp(\omega(\xi+1)^{-1/d}) C(\xi+1,\theta)] \\ &\quad + J\delta(\xi-\xi^*). \end{aligned} \tag{2.18}$$

The critical nucleus size and Gibbs–Thomson factor have the scaled forms

$$\xi^* = (\omega_d/\ln S)^d \quad \text{and } \Omega(\xi) = \omega_d/\xi^{1/d}. \tag{2.19}$$

3. Numerical solution

The problem of unsteady state nucleation, growth, and coarsening requires a numerical solution. Several numerical techniques have been reviewed [37,38] and the most common method that is used to solve PBE is the sectional method [39], wherein particles are assigned to different sections according to their volume. This method was extended by other investigators [40,41] to a 2-D sectional model in which agglomerate volume increased through coagulation. However, due to excessive computation time required for these methods, a modified sectional model [42,43] was developed, in which particles in each section were assumed to have the same size. Faster computations can be also achieved using 1-D sectional models [44,45], where it is assumed that the primary particle size is identical in a section. Recent computational methods such as the moving-sectional model [44] and fixed-sectional model [46] have been developed which are accurate and computationally efficient.

In this study, we use a numerical scheme similar to that developed previously [6]. While this computational technique may not be as computationally efficient as the techniques described above, CPU time of only 2 h on a Compaq AlphaServer ES40 is required to reach $\theta = 10^6$, by which time the asymptote is reached. The differential Eq. (2.18) was solved by a Runge-Kutta technique with an adaptive time step with $C(\xi, \theta)$ evaluated sequentially at each time step. At each time step, the mass balance (Eq. (2.17)) is verified to ensure accuracy of the numerical scheme. The particle moments were calculated by integration of the nonzero PSD from the critical particle size, ξ^* to ∞. Because $C(\xi, \theta)$ lies in the semi-infinite domain, it was converted to a bounded range (0,1) by the mapping function, $\xi = \xi^* + (C^{\text{avg}} - \xi^*)y/(1-y)$. When y varies from 0 to 1, ξ varies from ξ^* to ∞. By this mapping, when y is centered at 0.5, the distribution is centered around $C^{\text{avg}}(\theta)$ and is bounded at the lower end by ξ^*. The choice of this grid ensures that the mapping is fine in the range of prevalent sizes and coarse at very high and very low sizes. It is, therefore, possible to consider a narrow PSD with a few hundred intervals to do the numerical analysis. The mass variable (ξ) was divided into 1000 intervals and the adaptive time (θ) step varied from 0.001 to 0.1 ensuring stability and accuracy at all values of the parameters.

In the first step of the numerical routine, the concentration of all particles is zero and nuclei are generated at their critical size. The first terms on the right-hand sides of Eq. (2.18) are zero, so that the decrease of S and the increase of $C(\xi = \xi^*, \theta)$ can be determined. In the second step, the critical nucleus size has grown owing to the reduced value of S, but the particles evolving from the initial nuclei have also grown because of monomer deposition. All terms in Eq. (2.18) contribute to the computation. At each step of the iteration, particles smaller than the critical size instantaneously denucleate and transfer their mass to the uncondensed phase, an assumption that has been demonstrated by computations to be valid [16].

The choice of parameters is based in part on example calculations for water vapor nucleation [36] at 273 K where $\omega = 6.18$, and so we illustrate computations for $\omega = 4$–6. Values of initial supersaturation, S_0, influence the results significantly, such that $S_0 = 10$, 50, and 100 show good visual separation of the curves in our illustrative results. Because J depends exponentially on $-W^*/k_B T$, a slight increase in S causes a huge increase in the classical nucleation rate [36]. By contrast, the value of α in the prefactor influences J only linearly and, therefore, it is chosen to span two orders of magnitude, 0.01, 0.1, and 1.0. The remaining parameter that affects the computations is the power on mass in rate coefficient expressions and we choose $\lambda = 0$, $\frac{1}{3}$, and $\frac{2}{3}$, representing size-independent, diffusion-controlled and surface-controlled processes.

4. Results

As described above, the PSDs broaden initially and then narrow as coarsening occurs. The generic temporal behavior of supersaturation, $S(\theta)$, and Gibbs–Thomson factor, $e^{\Omega(\theta)}$, shows that both approach unity at long times with their difference being the driving force. The effects of entropy and energy driving forces in nucleation are governed

by the prefactor, $J_0 = \alpha S^2$, and the scaled exponential, $\exp[-W/k_B T] = \exp[-\omega^d (\ln S)^{1-d}/(d-1)]$, respectively, which are in turn related to α, ω, and S. As J is the time derivative of the particle number concentration [29], the transition time between nucleation-growth and coarsening occurs when $C^{(0)}$ is maximum.

The influence of four parameters, ω, S_0, α, and λ, on the time evolution of the PSD (or its moments) was determined. Figs. 2–5 show the effects of changing ω, S_0, α, and λ, respectively. The time when particle generation (nucleation) becomes particle loss (denucleation) is the principal marker in the transition from nucleation-growth to coarsening. The turnaround time occurs when $C^{(0)}(\theta)$ is maximum and hence $J = 0$. The number density maxima determine when maximum curvature appears for the average mass and polydispersity index (Figs. 2–5).

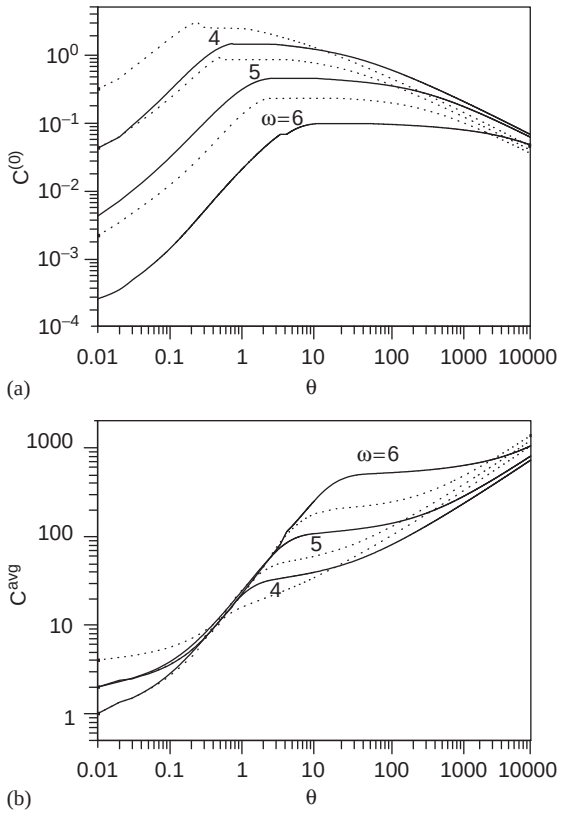

Fig. 2. Effect of ω on time dependence of (a) number concentration $C^{(0)}$ and (b) number average particle mass C^{avg}. Parameter values are $S_0 = 50$, $\alpha = 0.1$, and $\lambda = 0$. The dotted lines represent the cases for 3-D.

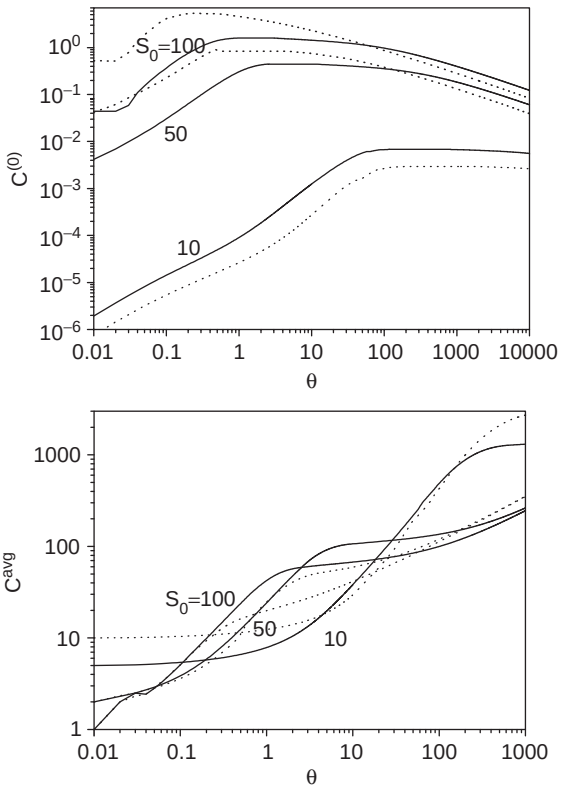

Fig. 3. Effect of the initial supersaturation S_0 on time dependence of number concentration $C^{(0)}$ and number average particle mass C^{avg}. Parameter values are $\omega = 5$, $\alpha = 0.1$, and $\lambda = 0$. The dotted lines represent the cases for 3-D.

A significant parameter controlling precipitate evolution is the interfacial energy, which influences both the nucleation rate (Eq. (2.14)) and critical nucleus size (Eq. (2.19)). In addition, interfacial energy also influences growth through the capillarity effect and drives the coarsening process. Fig. 2 shows the effect of ω on particle nucleation, growth, and coarsening. It can be seen that changing the interfacial energy has a marked effect on the shape of the number density evolution curves (Fig. 2a). At low interfacial energy values, there is no plateau when the number density reaches a constant. While an overlap between nucleation, growth, and coarsening always occurs, at low interfacial energies, the addition of new particles by nucleation effectively

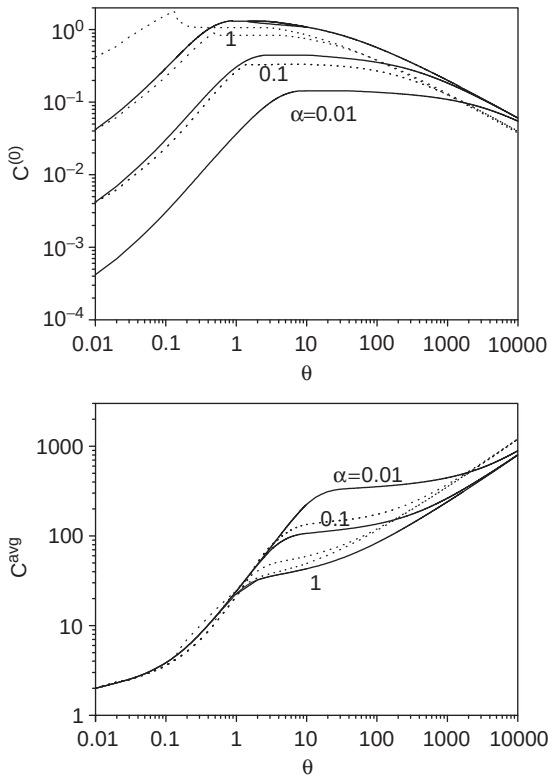

Fig. 4. Effect of the pre-exponential factor α on time dependence of number concentration $C^{(0)}$ and number average particle mass C^{avg}. Parameter values are $\omega = 5$, $S_0 = 50$, and $\lambda = 0$. The dotted lines represent the cases for 3-D.

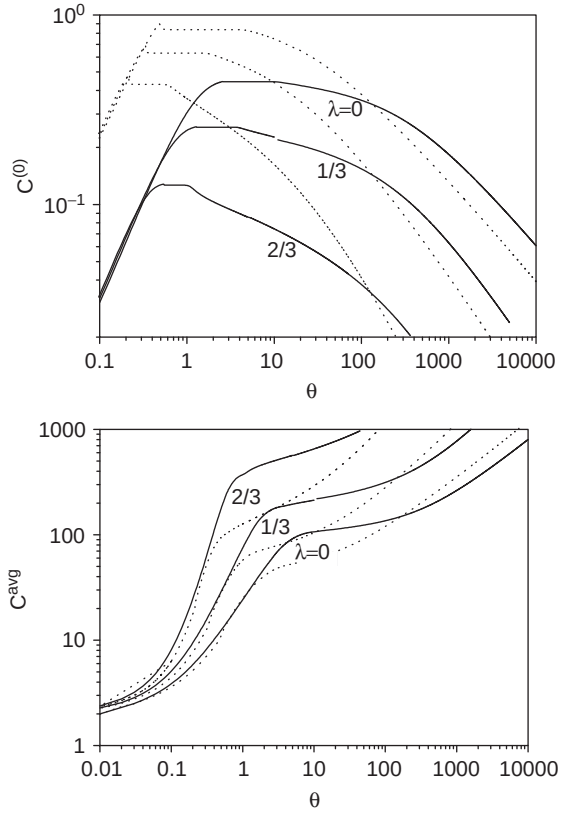

Fig. 5. Effect of the exponent λ on time dependence of number concentration $C^{(0)}$ and number average particle mass C^{avg}. Parameter values are $\omega = 5$, $S_0 = 50$, and $\alpha = 0.1$. The dotted lines represent the cases for 3-D.

ceases, and coarsening causes dissolution of the smallest particles, reducing the number density. A steady-state number density is, therefore, never obtained during precipitation at low interfacial energies. At higher interfacial energies, a plateau appears wherein the number density is nearly constant for some time. This corresponds to a case where there is a delay between the time at which the nucleation rate is nearly zero and the onset of a reduction in number density due to coarsening. The plateau is an extended time over which the mean particle radius increases while the critical radius increases slowly. When the interfacial energy is lowered, this plateau period is considerably reduced. Because the nucleation rate depends on the square of the supersaturation but depends exponentially on the interfacial energy, a small solute depletion results in a rapid reduction in the nucleation rate when the interfacial energy is high but there is still sufficient solute left for growth of all the precipitates. When the interfacial energy of the particle is low, however, a greater level of solute depletion can be tolerated before the rate of nucleation becomes negligible.

Supersaturation is an important parameter that determines the driving force for precipitation, and hence the nucleation and growth rates. Fig. 3 depicts how three values of initial supersaturation influence the process. In addition to a change in kinetics, a change in supersaturation changes the shape of the number density versus time plot. For low supersaturations, a plateau occurs at the maximum number density when there is no overlap between nucleation and coarsening. As the

supersaturation is increased, the plateau disappears when nucleation and coarsening start to overlap. Classical homogeneous nucleation is opposed by substantial denucleation, so that the overall nucleation rate is reduced. This occurs because as supersaturation declines, the critical nucleus size (Eq. (2.19)) increases faster than the particles growth. This is like the effect observed when the interfacial energy is increased and has similar origins. Nucleation is more sensitive to supersaturation than its growth. If the initial supersaturation is small, then even a small reduction in the solute level is sufficient to cause nucleation to become negligible. The coarsening, however, has not begun because many particles are below the critical size and there is no overlap of nucleation and coarsening. At large supersaturations, a significant nucleation rate is maintained even when a substantial proportion of the solute has been precipitated. This causes the critical radius to increase above the smallest particle size and coarsening begins, leading to an overlap of nucleation and coarsening. The effect of supersaturation and interfacial energies on the transition from nucleation to coarsening is consistent with the modified KWN model [18].

Fig. 4 shows the influence of prefactor α on the evolution of crystal size distribution. Homogeneous nucleation increases proportionately with α, producing the expected effects on the evolution of number and average particle size. According to our computations, the maximum can occur over a rather large time interval, thus separating the two stages from each other, as mentioned above. This explains why the onset of coarsening can be delayed significantly, and is therefore safely ignored for many precipitation or crystallization processes.

Fig. 5 shows how different values of λ determine the coarsening mode. Thus, $\lambda = 0$, $\frac{1}{3}$, or $\frac{2}{3}$ represent size-independent, diffusion-controlled, and surface-controlled coarsening, respectively, which shows that the onset of denucleation occurs sooner as λ increases.

Next, let us consider the effect of heterogeneous nucleation to show the asymptotic behavior. In the model, we assume that the critical size is the same for both homogeneous and heterogeneous nucleation. However, due to the shape factor, the volume of the critical nucleus will depend on the wetting angle and can be smaller for heterogeneous nucleation. We take $\omega = S_0 = 5$ and assume initial conditions such that the dimensionless zeroth moment $C_0^{(0)} = 1$ and the initial average particle mass $C_0^{\text{avg}} = 75$. Figs. 6a and b show the time evolution of the particle number concentration and average particle mass for various values of λ for 2- and 3-D systems for an initial delta distribution. The log–log plots indicate power-law decrease, $C^{(0)} \sim \theta^{-b}$, and increase, $C^{\text{avg}} \sim \theta^{b}$, with time. The polydispersity (not shown) always

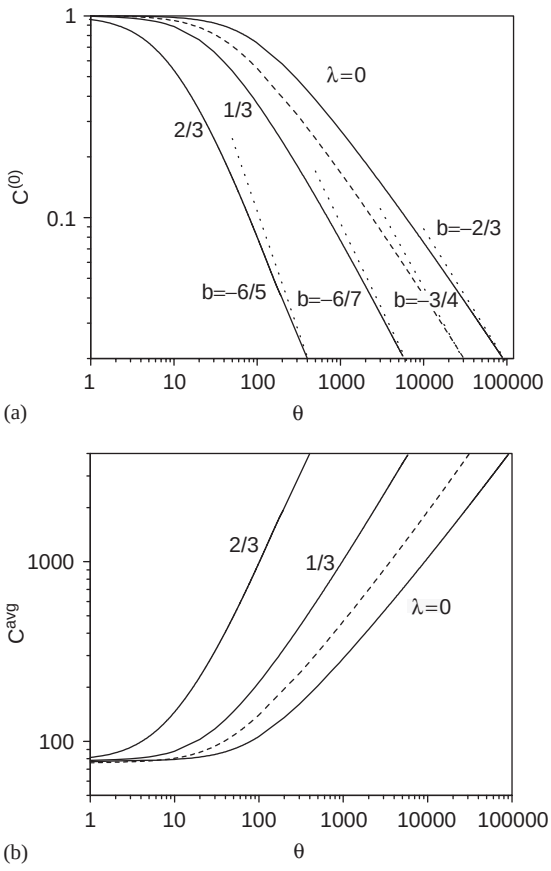

Fig. 6. Time evolution of the (a) particle number density, $C^{(0)}(\theta)$, and (b) average particle size, $C^{\text{avg}}(\theta)$, showing asymptotic power-law decrease with time for various λ. The parameters used in the calculations are $\omega = 5$, $S_0 = 5$, with $C_0^{(0)} = 1$ and initial delta distribution centered at $C_0^{\text{avg}} = 75$. The dashed line represents the case for 3-D. The dotted lines represent the asymptotic slopes given by $b = (1 - \lambda + 1/d)$.

approaches unity. It is obvious that the increase in average particle mass is caused by the decrease in number of particles. The power b approaches the long-time asymptotic value given by $(1-\lambda+1/d)^{-1}$, where d is the dimension. For $\lambda = 0$, the value of b is $\frac{2}{3}$ and $\frac{3}{4}$ for 2- and 3-D, respectively. Experimental techniques such as scanning tunneling microscopy (STM) and low-energy electron microscopy have been used to determine the asymptotic slope during the coarsening of homoepitaxial systems like Si(0 0 1) [47], Ag(1 1 1) [48], Ni(1 0 0) [49], and TiN(1 0 0) and TiN(1 1 1) [50], for which the clusters are one atom high islands. Asymptotic slopes of $-\frac{2}{3}$ and -1 were obtained for the decay of islands of TiN(0 0 1) and TiN(1 1 1), respectively. This is consistent with the asymptote predicted by our theory with $\lambda = 0$ and $\frac{1}{2}$.

Thus, the coarsening stage exhibits asymptotic power-law time dependence of the particle number concentration and average mass, with the polydispersity always approaching unity. The asymptotic analysis demonstrates that the long-time behavior is independent of the assumed values for initial number concentration $C_0^{(0)}$, initial average particle mass C_0^{avg}, initial supersaturation S_0, and also ω and α.

5. Conclusion

The temporal evolution of the PSD or its moments and of the supersaturation driving force is represented by a distribution kinetics approach based on PBEs for the particles and uncondensed monomer. Coarsening is accounted directly in the model. As the supersaturation decreases, the critical size of the particle increases and the driving force for growth decreases. The governing equations are solved numerically and it is shown that the transition from nucleation and growth to coarsening occurs over a relatively long time period. The previously reported overlap of nucleation, growth, and coarsening is confirmed by present results.

Four dimensionless parameters determine the evolution of a metastable uncondensed phase: the initial supersaturation S_0, the ratio of interfacial to thermal energy ω, the power on the rate coefficients λ, and the preexponential or frequency factor for nucleation α. The important quantity ξ^* is the critical (or stable) size of a particle in units of the monomer mass. Particles smaller than ξ^* are unstable and hence vanish spontaneously. The reason that metastable phases can exist is that an energy barrier must be surmounted for particles to become stable and hence to grow by monomer deposition. Homogeneous nucleation theory prescribes the rate of formation of stable nuclei of size ξ^*. Coarsening exhibits asymptotic power-law time dependence for decrease in particle number density and increase in average particle mass. The asymptotic coarsening stage shows a power-law increase in average particle mass as the PSD evolves to a delta distribution with zero variance for both 2- and 3-D phase transitions.

References

[1] J.A. Marqusee, J. Ross, J. Chem. Phys. 79 (1983) 373.
[2] R.B. McClurg, R.C. Flagan, J. Colloid Interface Sci. 201 (1998) 194.
[3] B.J. McCoy, J. Colloid Interface Sci. 240 (2001) 139.
[4] B.J. McCoy, I&EC Res. 40 (2001) 5147.
[5] G. Madras, B.J. McCoy, J. Chem. Phys. 115 (2001) 6699.
[6] G. Madras, B.J. McCoy, J. Chem. Phys. 117 (2002) 8042.
[7] W. Ostwald, Z. Phys. Chem. 34 (1900) 495.
[8] I.M. Lifshitz, V.V. Slyozov, J. Phys. Chem. Solids 19 (1961) 35.
[9] C. Wagner, Z. Elektrochem. 65 (1961) 581.
[10] W.J. Dunning, Ripening and ageing processes in precipitates, in: A.L. Smith (Ed.), Particle Growth in Suspensions, Academic Press, New York, 1973.
[11] W.W. Mullins, J. Appl. Phys. 59 (1986) 1341.
[12] B.K. Chakraverty, J. Phys. Chem. Solids 28 (1967) 2401.
[13] B.J. McCoy, G. Madras, Chem. Eng. Sci. 56 (2001) 2831.
[14] H. Xia, M. Zinke-Allmang, Physica A 261 (1998) 176.
[15] G. Madras, B.J. McCoy, Phys. Chem. Chem. Phys. 5 (2003) 5459.
[16] G. Madras, B.J. McCoy, J. Chem. Phys. 117 (2002) 6607.
[17] R. Kampmann, R. Wagner, in: P. Haasen, V. Gerold, R. Wagner, M.F. Ashby (Eds.), Decomposition of Alloys, the Early Stages, Pergamon Press, Oxford, 1984, p. 91.
[18] J.D. Robson, Acta Mater. 52 (2004) 4669.
[19] P. Mirold, K. Binder, Acta Mater. 25 (1977) 1435.
[20] V.V. Slezov, J. Schmelzer, Y.Y. Tkatch, J. Chem. Phys. 105 (2002) 8042.
[21] W.J. Dunning, Ripening and ageing processes in precipitates, in: A.L. Smith (Ed.), Particle Growth in Suspensions, Academic Press, New York, 1973.
[22] A. Onuki, Phase Transition Dynamics, Cambridge University Press, Cambridge, UK, 2002.

[23] R. Kampmann, R. Wagner, Materials Science and Technology, vol. 5, VCH–Weinheim, Germany, 1991.
[24] J.D. Robson, M.J. Jones, P.B. Prangnell, Acta Mater. 51 (2003) 1453.
[25] J.D. Robson, Mater. Sci. Technol. 20 (2004) 441.
[26] G. Madras, B.J. McCoy, J. Colloid Interface Sci. 261 (2003) 423.
[27] G. Madras, B.J. McCoy, Acta Mater. 51 (2003) 2031.
[28] G. Madras, B.J. McCoy, J. Crystal Growth 243 (2002) 204.
[29] G. Madras, B.J. McCoy, Chem. Eng. Sci. 57 (2002) 3809.
[30] G. Madras, B.J. McCoy, J. Chem. Phys. 119 (2003) 1683.
[31] M. Abramowitz, I.A. Stegun, Handbook of Mathematical Functions, National Bureau of Standards, 1968 (Chapter 26).
[32] D.F. Calef, J.M. Deutch, Ann. Rev. Phys. Chem. 34 (1983) 493.
[33] K. Binder, Phys. Rev. B 15 (1977) 4425.
[34] H. Gratz, Scr. Mater. 18 (1997) 1637.
[35] H. Dobberstein, R.W. Schwartz, Proceedings of the First Symposium on Advanced Materials for Next Generation—Prelude to Functional-Integrated Materials, AIST Chubu, Nagoya, Japan, May 27, 2002.
[36] A.W. Adamson, A.P. Gast, Physical Chemistry of Surfaces, sixth ed., Wiley-Interscience, New York, 1997.
[37] D. Ramkrishna, Rev. Chem. Eng. 3 (1985) 49.
[38] Y. Zhang, C. Seigneur, J.H. Seinfeld, M.Z. Jacobson, F.S. Binkowski, Aerosol Sci. Technol. 31 (1999) 487.
[39] F. Gelbard, Y. Tambour, J.H. Seinfeld, J. Colloid Interface Sci. 76 (1980) 541.
[40] Y. Xiong, S.E. Pratsinis, J. Aerosol Sci. 24 (1993) 283.
[41] K. Nakaso, T. Fujimoto, T. Seto, M. Shimada, K. Okuyama, M.M. Lunden, Aerosol Sci. Technol. 35 (2001) 929.
[42] M.J. Hounslow, R.L. Ryall, V.R. Marshall, A.I.Ch.E. J. 34 (1988) 1821.
[43] S. Kumar, D. Ramkrishna, Chem. Eng. Sci. 52 (1997) 4659.
[44] S. Tsantilis, H.K. Kammler, S.E. Pratsinis, Chem. Eng. Sci. 57 (2002) 2139.
[45] S.H. Park, S.N. Rogak, Aerosol Sci. Technol. 37 (2003) 947.
[46] S.H. Park, S.N. Rogak, J. Aerosol Sci. 35 (2004) 1385.
[47] N.C. Bartelt, W. Theis, R.M. Tromp, Phys. Rev. B. 54 (1996) 11741.
[48] K. Morgenstern, G. Rosenfeld, G. Comsa, Surf. Sci. 441 (1999) 289.
[49] M.S. Hoogeman, M.A.J. Klik, R. van Gastel, J.W.M. Frenken, J. Phys.: Condens. Matter 11 (1999) 4349.
[50] S. Kodambaka, V. Petrova, A. Vailionis, P. Desjardins, D.G. Cahill, I. Petrov, J.E. Greene, Thin Solid Films 392 (2001) 164.